CO internal excitation from the reaction: $H+CO_2 \rightarrow CO+OH$

Scott L. Nickolaisen, Harry E. Cartland,[a] and Curt Wittig
Department of Chemistry, University of Southern California, Los Angeles, California 90089-0482

(Received 14 February 1991; accepted 10 December 1991)

Time-resolved infrared diode laser absorption spectroscopy has been used to probe CO internal excitation following 193 nm photolysis of 300 K H_2S/CO_2 samples. Vibrations and rotations are colder than statistical, i.e., E_{int} (CO) is only $\sim 1500\ cm^{-1}$ even though $\sim 10\,000\ cm^{-1}$ is available for product excitations, assuming modest collisional deactivation of the hot H atoms that undergo reaction. A $[v=1]/[v=0]$ ratio of ~ 0.4 is obtained and there is essentially no population at $v \geqslant 2$. Both the $v=0$ and 1 rotational distributions are cold, peaking at $J_{max} \sim 11$ and 13, respectively. The vibrational distribution is nascent while the rotational distributions may be partially relaxed, but not enough to alter the main conclusions. Combined with earlier results for OH internal excitations and center-of-mass (CM) kinetic energies, we conclude that at high collision energies there is a propensity toward product CM kinetic energy. In this regime, the reaction cross section rises rapidly with energy and statistical unimolecular rate theory is not applicable, even with a $HOCO^{\dagger}$ intermediate.

I. INTRODUCTION

The reaction of hydrogen atoms with carbon dioxide

$$H + CO_2 \rightarrow CO + OH \quad \Delta H_{298} = 8960\ cm^{-1} \qquad (1)$$

has been studied thoroughly both experimentally and theoretically (see Fig. 1).[1-10] Interest derives from several factors. The reverse reaction is the predominant pathway for the formation of carbon dioxide in the combustion of hydrogenous systems,[11] and plays a role in the upper-atmosphere chemistry of HO_x species.[12] Also, because the system involves only light elements, an accurate *ab initio* potential energy surface can be calculated, checked against thermochemical data, and used in dynamical studies that model the many experimental results. Thus this system enables an excellent comparison to be made between experiment and current dynamical theories.

Many studies of reaction (1) have used photolytically prepared H atoms and have detected nascent OH by laser-induced fluorescence (LIF). The first was by Quick and Tiee[1] at a center-of-mass (CM) collision energy of 2.6 eV, in which OH was measured in $v=0$, 1, and 2 following 193 nm HBr photolysis. Kleinermanns *et al.*[2] subsequently measured $v=0$ rotational distributions for both 1.9 and 2.6 eV collision energies. The distributions peaked at $J_{max} \sim 7$ and 11, respectively, and both were colder than statistical with rotational surprisal parameters of $\theta_R = 2.8 \pm 0.3$ (Ref. 2). Jacobs *et al.* determined a reaction cross section of 0.4 ± 0.2 Å^2 for 1.9 eV collisions.[3] Radhakrishnan *et al.* found that the $v=0$ and 1 rotational distributions deriving from photoexcited CO_2–HBr complexes were colder than for 300 K bulk (i.e., single-collision, arrested-relaxation) conditions and obtained $[v=1]/[v=0] \sim 0.4$ (Ref. 4). Rice *et al.* then measured OH distributions following 193 nm H_2S photolysis under both bulk and complexed conditions, the former yielding a $v=0$ distribution with $J_{max} \sim 6$ for 300 K samples.[5] Cooling the sample in an uncomplexed expansion (i.e., low-temperature bulk conditions) left the OH distributions unchanged. With CO_2–H_2S complexes, however, OH rotational excitation was reduced markedly ($J_{max} \sim 2$). Scherer *et al.* measured the appearance of OH using a picosecond pump–probe system, in which the precursor was the CO_2–HI complex and the quantity $h\nu - D_0$ was varied from 1.79 to 2.20 eV.[6] The rising portions of the time-resolved signals were fit using an exponential function with two time constants, the smaller ranging from 0.7 to 1.2 ps and the larger ranging from 1.1 to 4.4 ps as $h\nu - D_0$ was varied from 2.20 to 1.79 eV. These measurements confirmed the role of an intermediate as opposed to a rapid stripping process.

CO distributions have been reported by Rice *et al.*, who used vuv LIF to measure the $v=0$ and 1 rotational distributions following 193 nm H_2S photolysis.[7] For 300 K bulk conditions, they found $J_{max} \sim 13$ for $v=0$, while for low-temperature bulk conditions, J_{max} for $v=0$ was seen to decrease by a few quanta depending on the expansion temperature. They also reported $J_{max} \sim 26$ for $v=1$, with an inverted rotational distribution. The $v=0$ and 1 concentrations were estimated to be comparable when using 300 K samples.

Schatz, Fitzcharles, and Harding (SFH) calculated the HOCO potential surface using *ab initio* techniques.[8(a)] Once a global surface was fit, trajectories were run in which the CM kinetic energy, E_{CM}, was either 1.9 or 2.6 eV. At $E_{CM} = 2.6$ eV they found $\langle v_{CO} \rangle = 1.2$, $\langle J_{CO} \rangle = 25$, $\langle v_{OH} \rangle = 0.5$, $\langle J_{OH} \rangle = 11$. Aoyagi and Kato also calculated the potential surface *ab initio*,[8(b)] and were able to fit thermally averaged data over a wide temperature range using RRKM theory.

In the present study, results of reactive collisions at $E_{CM} \leqslant 2.4$ eV are reported, with product CO monitored state selectively. Section II describes the experimental arrangement in which hot H atoms were generated by 193 nm H_2S photolysis, and CO product was monitored by time resolved ir absorption spectroscopy using a tunable diode laser probe. Section III outlines the model used to extract V,R distributions from the absorption signals; rotational distributions for $v=0$ and 1 are presented and are fit to surprisal parameters.

[a] Science Research Laboratory, U. S. Military Academy, West Point, New York 10996.

 0021-9606/92/064378-09$06.00

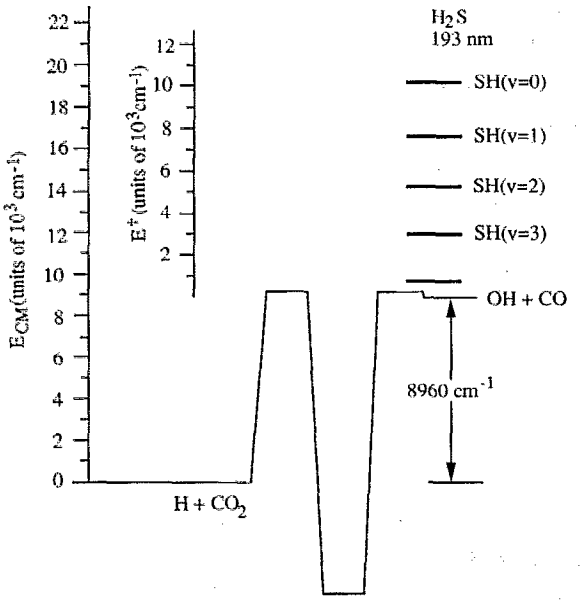

FIG. 1. Reaction coordinate diagram for the HOCO system showing CM collision energies appropriate to the experiments. For nascent H atoms deriving from 193 nm H_2S photolysis, different SH vibrational levels correspond to different H-atom speeds.

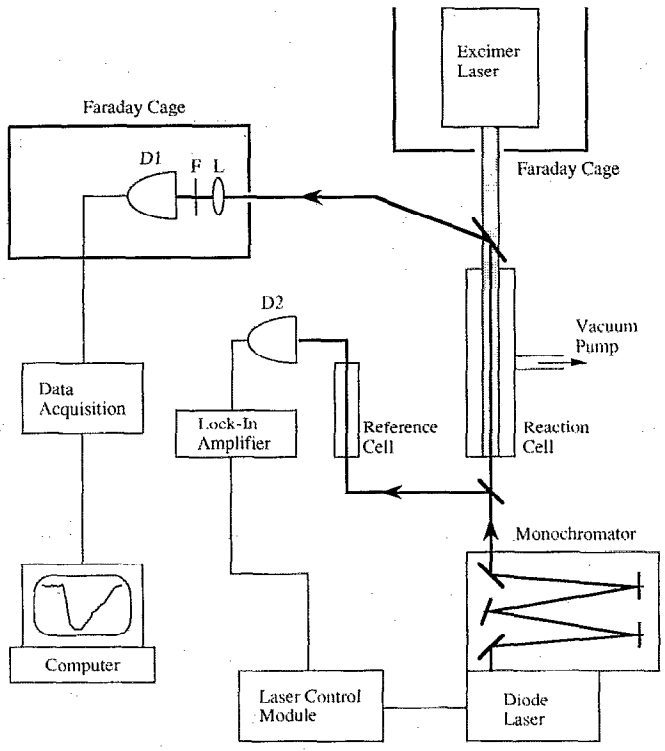

FIG. 2. Schematic of experimental arrangement. D_1 is a 0.25 mm×0.25 mm InSb detector; D_2 is a 1 cm×1 cm InSb detector; F is two 3.5–6.5 μm bandpass filters; L is a 10 cm f.l. CaF_2 lens.

Section IV examines the SFH surface and discusses factors that may influence energy disposal. A summary is given in Sec. V.

II. EXPERIMENTAL

The experimental arrangement is shown schematically in Fig. 2. The reaction cell was a 190 cm by 15 cm diam. stainless steel tube with MgF_2 windows. Gas mixtures were introduced at the ends of the cell and evacuated with a mechanical pump. A mixture of 20% H_2S (Matheson, 99.5%) in CO_2 (MG Industries, 99.8%) was premixed and flowed through the cell at a rate of approximately 1.4 ℓs^{-1} at a total pressure of 200 mTorr. Because the excitation volume was small relative to the cell volume, it was not necessary to completely flush the cell of reactive products between laser firings at the 10 Hz repetition rate.

Hydrogen atoms were prepared by 193 nm excimer laser photolysis of H_2S. The excimer laser (Lambda Physik, EMG 201) was enclosed in a Faraday cage to reduce rf interference. Steering of the uv beam was done with fused silica prisms. The uv beam was passed through a 1 cm iris in front of the reaction cell resulting in a total irradiated volume of 150 cm^3, which is small compared to the 34 000 cm^3 volume of the cell. 193 nm H_2S photolysis produces H atoms with a distribution of kinetic energies, corresponding to vibrational excitation of the HS fragment. Namely, 68% of the H atoms produced have a kinetic energy of 2.4 eV in the H + CO_2 CM system, corresponding to SH($v=0$). The remainder are associated with a number of SH vibrational states, corresponding to lower CM kinetic energies.[13]

The distribution of CM kinetic energies needs to be multiplied by the relative rates of reaction, which increase steeply with collision energy in this region, to obtain the distribution for *reacting* H atoms. Collision energies and reaction cross sections are shown in Fig. 3 for the case of nascent H atom speeds. Although only 68% of the H atoms have the maximum collision energy of 19 170 cm^{-1}, approximately 96% of the *reactive* H atoms have this kinetic energy (see

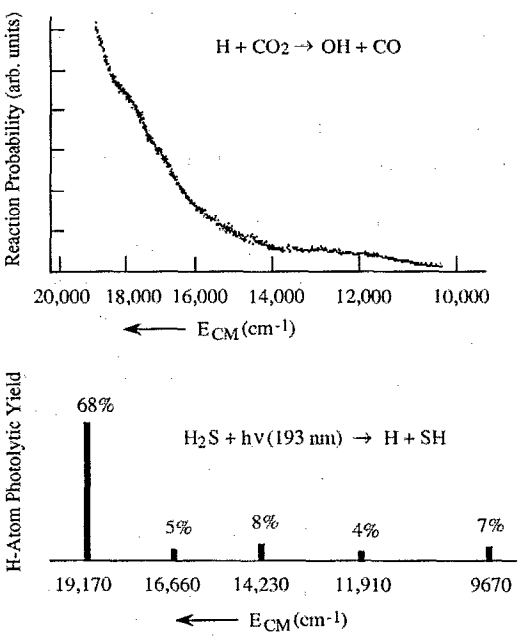

FIG. 3. (upper) Reaction probability vs E_{CM}, showing the marked increase with E_{CM}; (lower) distribution of H-atom speeds from 193 nm H_2S photolysis; only those in excess of ΔH are shown.

TABLE I. H-atom distribution and $H + CO_2$ CM collision energies deriving from 193 nm H_2S photolysis (single collision conditions). The relative amounts of reactive H atoms (last column) are proportional to the reaction rate times the nascent H-atom concentrations produced by H_2S photolysis (see Fig. 3). Note the bias toward high collision energies brought about by the steep variation of the reaction rate with collision energy.

v(SH)	E_v(SH) (cm^{-1})	E_{CM} (cm^{-1})	$[H]/[H]_{total}$	k_1 (arb. units)	$k_1[H]/[H]_{total}$ (normalized to unity)
0	0	19 170	0.68	14.4	0.964
1	2 647	16 660	0.05	5.7	0.024
2	5 198	14 230	0.08	1.5	0.009
3	7 651	11 910	0.04	1.0	0.002
4	10 007	9 670	0.07		
5	12 267	7 530	0.05		
6	14 429	5 470	0.02		
7	16 494	3 510	0.01		

Table I). Thus the experiment is biased toward the highest collision energies.

CO was monitored using an infrared tunable diode laser (Laser Analytics, SP5740) with a beam diameter of ~0.5 cm. Laser mode and coarse wavelength selection were accomplished with a 0.5 m monochromator (Laser Analytics, SP5151). The ir beam was split with a coated Ge flat and ~60% was directed through the reaction cell; the remainder passed through a reference cell which provided exact wavelength calibration. It was necessary to monitor CO in $v = 1$ as well as $v = 0$ to obtain the $v = 0$ population, since absorption spectroscopy measures population differences. Therefore, $v = 1$ was generated in a reference cell by maintaining a glow discharge in a water-cooled Pyrex vessel sealed at the ends with CaF_2 windows. The discharge was stabilized with a constant-current control circuit that enabled the current to be adjusted independently of the high voltage setting. A mixture of ~0.5 Torr CO (MG Industries, 99.5%) and ~2 Torr He (MG Industries, 99.999%) was flowed through the reference cell (typically 5 kV and 5 mA). The reference beam was monitored with an InSb photovoltaic detector (Spectronics, 1 cm^2, response time ~1 μs).

Using this reference configuration, CO in both $v = 0$ and $v \geqslant 1$ could be monitored. The TDL output was locked to a CO transition line center using the internal function generator of the laser control module to obtain a 2.5 kHz triangle wave superimposed on the TDL current. The triangle wave amplitude was adjusted to correspond to a dither of 0.015 cm^{-1} in the TDL output. The output of the reference detector preamplifier was connected to a lock-in amplifier whose phase was adjusted to produce a first derivative signal of the reference detector output. The lock-in output was attenuated by a factor of 100 and connected to the external current input of the laser control module. This feedback scheme produced a correction signal that locked the TDL wavelength to the center of the desired transition.

The ir probe beam was separated from the uv beam by a quartz flat mounted at an angle of 23° to the uv path. Signals were obtained with an InSb photovoltaic detector (Santa Barbara Research Center, EC63) having a 0.25 mm×0.25 mm active area. The ir beam was focused onto the detector with a CaF_2 lens, and filtered from reflected uv and visible light by two 3.5–6.5 μm bandpass filters. The output of the detector preamplifier (Perry, 750) was connected to a unity gain line driver (Perry, 491-50). The detector, preamplifier, and line driver were all contained within a Faraday cage. The signal was amplified by a 40 dB, 200 Hz–60 MHz voltage amplifier and filtered by a 7.1 kHz–4.8 MHz bandpass filter. The response time of the detector and amplifier combination was 250 ns. The signal output was connected to a 10^8 samples s^{-1} transient digitizer. Signal averaging was performed by the crate controller, and the data acquisition hardware was controlled using drivers written in the ASYST language which were developed in this laboratory. Averaged signals were transferred to a computer for storage and analysis. The timing of the excimer-laser and transient-digitizer triggers was controlled by a dual channel master clock. Data were collected at 10 Hz, and 1500 transients were typically averaged for each wave form.

An analytical fit to the SFH surface was provided by Schatz.[8(a)] The energy of the separated, ground state $H + CO_2$ reactants was assigned the value zero. In most cases, the geometry of the OCO "molecule" was fixed, and the H atom was moved along constant energy lines to produce contour maps. Analogous contours for the reacting O atom were obtained by fixing the positions of the other atoms and moving the O atom.

III. RESULTS

To interpret the transient absorption signals, a model is needed that includes the relevant formation, energy transfer, and removal processes involved in the temporal evolution of $CO(v,J)$ concentrations. Many of these processes are listed below in simplified form,

$$H_2S + h\nu(193\text{nm}) \rightarrow H^* + SH, \quad (2)$$
$$H^* + CO_2 \rightarrow CO(v,J) + OH, \quad (3a)$$
$$H^* + CO_2 \rightarrow CO(v',J') + OH, \quad (3b)$$
$$H^* + CO_2 \rightarrow H + CO_2, \quad (4)$$
$$H^* + H_2S \rightarrow H_2 + SH, \quad (5)$$
$$H^* + H_2S \rightarrow H + H_2S, \quad (6)$$
$$H^* \rightarrow \text{travels out of observation region}, \quad (7)$$
$$\Sigma_{v'J'} CO(v',J') + M \rightarrow CO(v,J) + M, \quad (8a)$$
$$CO(v,J) + M \rightarrow \Sigma_{v''J''} CO(v'',J'') + M, \quad (8b)$$

where H* refers to translationally hot H atoms. Reaction

(3a) is the reaction of interest, producing a specific $CO(v,J)$ level.

The physical situation behind Eqs. (2)–(8) is complicated and extracting information from the observed transient signals requires care. Fortunately, the probability of reaction (3) varies strongly with collision energy as shown in Fig. 3. Namely, collisionally deactivated H atoms undergo a loss of reactivity, thus biasing observations toward reflecting the highest hydrogen atom speeds. Since some collisional deactivation of hot H atoms inevitably occurs, we cannot accurately assign the experimental collision energies, although such quenching favors contributions from nascent reactants. It is also possible to separate the production and removal rates for the probed $CO(v,J)$ levels. Even though state-to-state rotational energy transfer cross sections are large, our measurements are sensitive only to *net* changes in the concentrations being monitored. The decay times of the transients are relatively slow compared to the risetimes, with the production of CO manifest in the risetimes. Details are given below.

By modeling CO rotational energy transfer as a two-level process in which exchange occurs between the monitored $CO(v,J)$ level and a "bath" level, an expression for the time-dependent $CO(v,J)$ concentration can be derived

$$[CO(v,J)](t) = \frac{[H^*]_0[CO_2]\{k_{3a} - \tau_r(k_{3a}+k_{3b})k_{8a}[M]\}}{\{\tau_r^{-1} - \tau_8^{-1}\}}\{\exp(-t/\tau_8) - \exp(-t/\tau_r)\}$$
$$+ \tau_r\tau_8(k_{3a}+k_{3b})k_{8a}[M][H^*]_0[CO_2]\{1-\exp(-t/\tau_8)\}, \quad (9)$$

where $\tau_r^{-1} = \{(k_{3a}+k_{3b}+k_4)[CO_2] + (k_5+k_6)[H_2S] + k_7\}$, and $\tau_8^{-1} = (k_{8a}+k_{8b})[M]$. The rate constant for reaction (3) is given by $k_3 = \Sigma\sigma_i v_i$, where σ_i is the reactive cross section at v_i. A maximum cross section for nascent H atoms of ~ 2 Å^2 is determined by interpolating the data shown in Fig. 3.[10,14] However, the value calculated from trajectories on the SFH surface is ~ 0.3 Å^2.[8] This large difference makes it impossible to accurately determine the contribution of reaction (3) to τ_r^{-1}, although it provides a range of $3\text{–}20\times 10^2$ s^{-1}.

In the present experiments, the mean free path of nascent H atoms is ~ 1 mm, i.e., less than the probe beam diameter. Some collisions of H atoms with CO_2 will be elastic with only the direction of the velocity altered, resulting in diffusion of hot H atoms out of the probed volume. For the cylindrically symmetric geometry of overlapped laser beams, the hot H atom concentration drops to e^{-1} of its original value within the probe beam in $\sim 5\,\mu$s. Thus the diffusion contribution lies near the low end of the estimated range for reaction (3) contribution.

We must also consider inelastic scattering in which CO_2 and H_2S vibrational and rotational levels are excited. Flynn *et al.* have examined such processes in detail for CO_2.[16] Although the total inelastic cross section has not been measured, calculations on the SFH surface suggest it is much larger than the reactive cross section.[8a] A principal effect of inelastic collisions is to lower the reaction probability by lowering the $H + CO_2$ collision energy, as shown in Fig. 3. For example, collisional excitation of $CO_2(001)$ reduces the reaction probability of the inelastically scattered H atoms to $\sim 1/3$ the value for nascent H atoms. Unfortunately, absolute cross sections for such processes are not accurately known and there are discrepancies between experimental and theoretical values for both reactive and inelastic scattering cross sections.[3,8,14,16] Thus it is not possible to quantify the overall contribution of inelastic scattering to τ_r^{-1}, although it will exceed that of reaction (3). The variation shown in Fig. 3 discriminates against H atoms that have been slowed by inelastic scattering.

The rate constant for $H + H_2S \rightarrow H_2 + SH$ is approximately 1.7×10^{-11} cm^3 molecule^{-1} s^{-1} at the present collision energies.[17] Thus this process does not contribute significantly.

Since the rate for $CO(v=1)$ vibrational relaxation by CO_2 is 4 orders of magnitude less than the collision frequency, it can be neglected.[18] However, CO/CO_2 rotational energy transfer rates have not been measured, and nascent CO has an average speed of $\sim 10^5$ cm s^{-1} and a collision frequency of $\sim 2\times 10^6$ assuming a 30 Å^2 cross section. Even if state-to-state rotational energy transfer rates are gas kinetic, what we observe is the *net change in level populations*. These can vary more slowly than state-to-state rates because population is transferred both out of and into the probed levels. This can be observed in the transient absorption signals (see Fig. 4). The rise is linear for over 1 μs following photolysis and decays with a longer time constant, attributed to relaxation into and out of the pair of states involved in the transition. Thus the distributions we report reflect some rotational relaxation, but we believe not enough to alter the conclusions.

The above considerations lead to an expression for the $CO(v,J)$ density at short times

$$[CO(v,J)](t) = \{k_3(v,J)[H^*]_0[CO_2]\}\cdot t. \quad (10)$$

The state-specific rate coefficients, $k_3(v,J)$, are proportional to the initial slope of $[CO(v,J)]$ vs t. Thus signals such as those shown in Fig. 4 were fit to straight lines for about 1 μs following excimer laser firing to obtain values of $k_3(v,J) - k_3(v,'J')$

$$\text{Signal} \propto [CO(v,J)] - [CO(v',J')]$$
$$= \{k_3(v,J) - k_3(v',J')\}[H^*]_0[CO_2]\cdot t. \quad (11)$$

Since we find no population with $v \geqslant 2$, the $v=0$ and 1 populations were obtained straightforwardly: $2\leftarrow 1$ transitions yield $k(1,J)$ values and $1\leftarrow 0$ transitions then yield $k_3(0,J)$ values. Results are shown in Fig. 5. The main assumptions are (i) Doppler widths do not change appreciably from one transition to the next, (ii) CO spatial anisotropy can be ne-

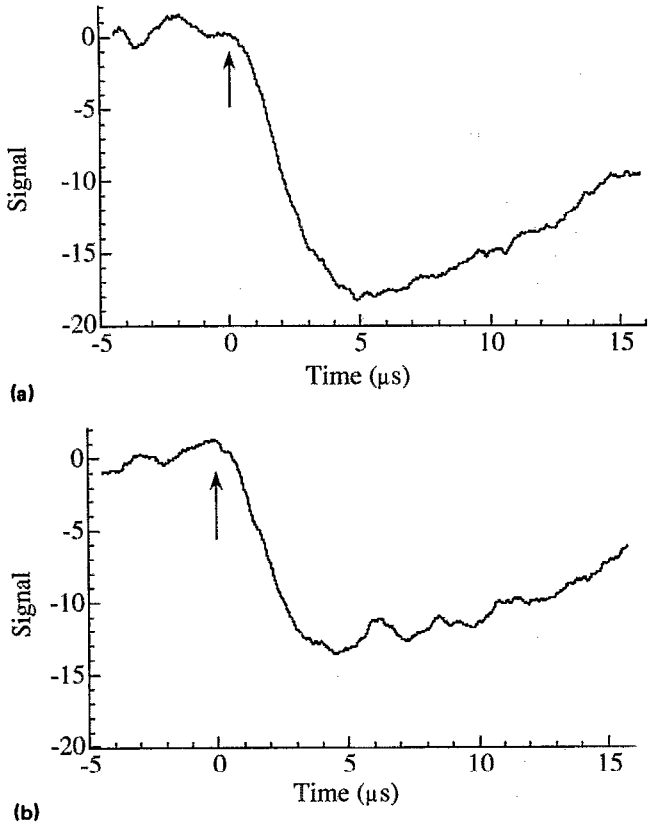

FIG. 4. Transient ir absorption signals: (a) $1\leftarrow0$ $R(10)$; (b) $2\leftarrow1$ $R(16)$. Negative signal indicates absorption. The vertical axis is in the same arbitrary units for each plot.

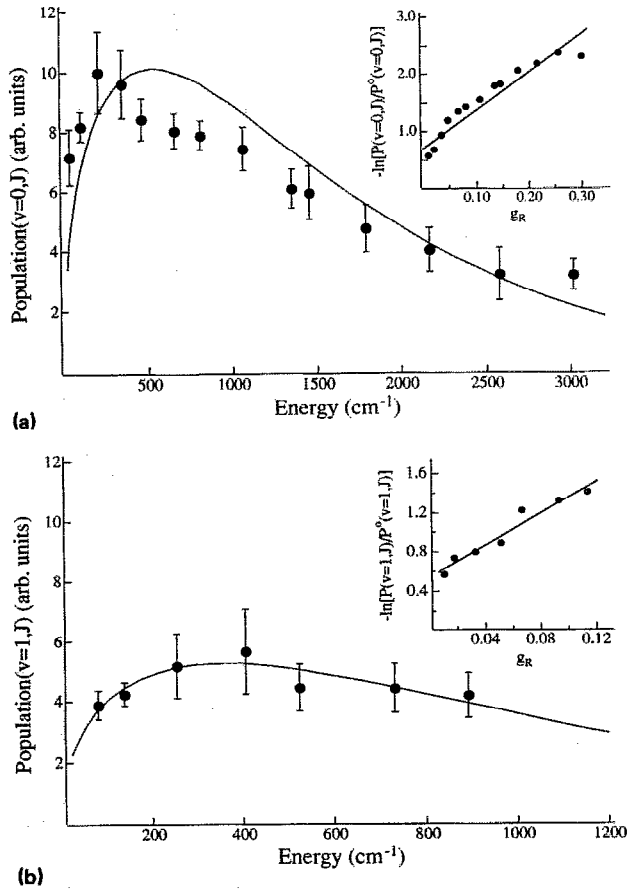

FIG. 5. CO rotational distributions for (a) $v=0$ and (b) $v=1$. Solid lines are from surprisal analyses (upper right inset); $\theta_R=7$ and 9 for $v=0$ and 1, respectively.

glected, (iii) net CO rotational relaxation is slower than the sum of the rates for hydrogen diffusion, reactive scattering, and inelastic scattering, and (iv) vibrational levels with $v\geqslant2$ are unpopulated. The Doppler width assumption is justified because most of the available energy goes into CM translation, so changes in the CO state being monitored and/or the corresponding OH internal states do not alter the Doppler width enough to warrant corrections at the present S/N. The assumption of no CO spatial anisotropy is justified in terms of the limited S/N and small anisotropies characteristic of such systems.

Most of the uncertainty is due to modest S/N and repeatability (see Fig. 4). Initial slopes were fit to straight lines using a least squares routine and were normalized for uv photolysis energy and ir probe power. Thus by measuring such traces for a range of $1\leftarrow0$ and $2\leftarrow1$ rotational transitions, the distributions shown in Fig. 5 were determined.

The data were also fit to Lagrange multipliers that constrain the energy entering the CO rotational degree of freedom, i.e., the approach developed by Levine, Bernstein, and co-workers.[19] Using continuous functions for translation and rotation and counting vibrations directly, the Prior distributions are given by

$$P^0(v,J)=(2J_{\rm CO}+1)\sum_{v(\rm OH)}\{1-f_V^{\rm OH}-f_V^{\rm CO}-f_R^{\rm CO}\}^{3/2}, \tag{12}$$

where $f_V^{\rm OH}$ is the fraction of the total energy in the OH vibrational degree of freedom, and so forth. The solid lines superimposed on the data shown in Fig. 5 are the rotational distributions resulting from surprisal analyses of the experimentally determined populations, $P(v,J)$. The surprisal plots (i.e., $-\ln[P(v,J)P^0(v,J)]$ vs the fraction of the available energy in rotation, g_R) are shown as insets in Fig. 5. The large positive surprisal parameters ($\theta_R=7$ for $v=0$ and $\theta_R=9$ for $v=1$) indicate substantial bias against CO rotation. The fit for CO($v=0$) is not good, but still indicates significant bias. The most probable rotational levels for $v=0$ and 1 are $J_{\rm max}=11$ and 13, respectively. The $[v=1]/[v=0]$ ratio was estimated by integrating the area under the rotational distribution for each vibrational state and resulted in $[v=1]/[v=0]\sim0.4$. These results and those of Rice *et al.* are summarized in Table II.

TABLE II. CO $v=0$ and 1 relative populations; results of Rice and coworkers are in parentheses (Ref. 7). $J_{\rm max}$ refers to the peak of the rotational energy distribution; θ_R is a surprisal parameter.

v	$J_{\rm max}$	θ_R	Rel. population
0	11 (12)	7.2	1.0 (1.0)
1	13 (23)	9.0	0.4 (1.0)

$\langle E_{\rm int}({\rm CO})\rangle=1540$ (2070) cm^{-1}

IV. DISCUSSION

The reaction of hydrogen atoms with carbon dioxide proceeds via a HOCO intermediate. It is impossible for the light H atom to simply strip away an O atom as it flies past. The H atom must slow considerably, and while this necessarily involves an "intermediate," it does not insure a statistical unimolecular decomposition mechanism.[20] The energy

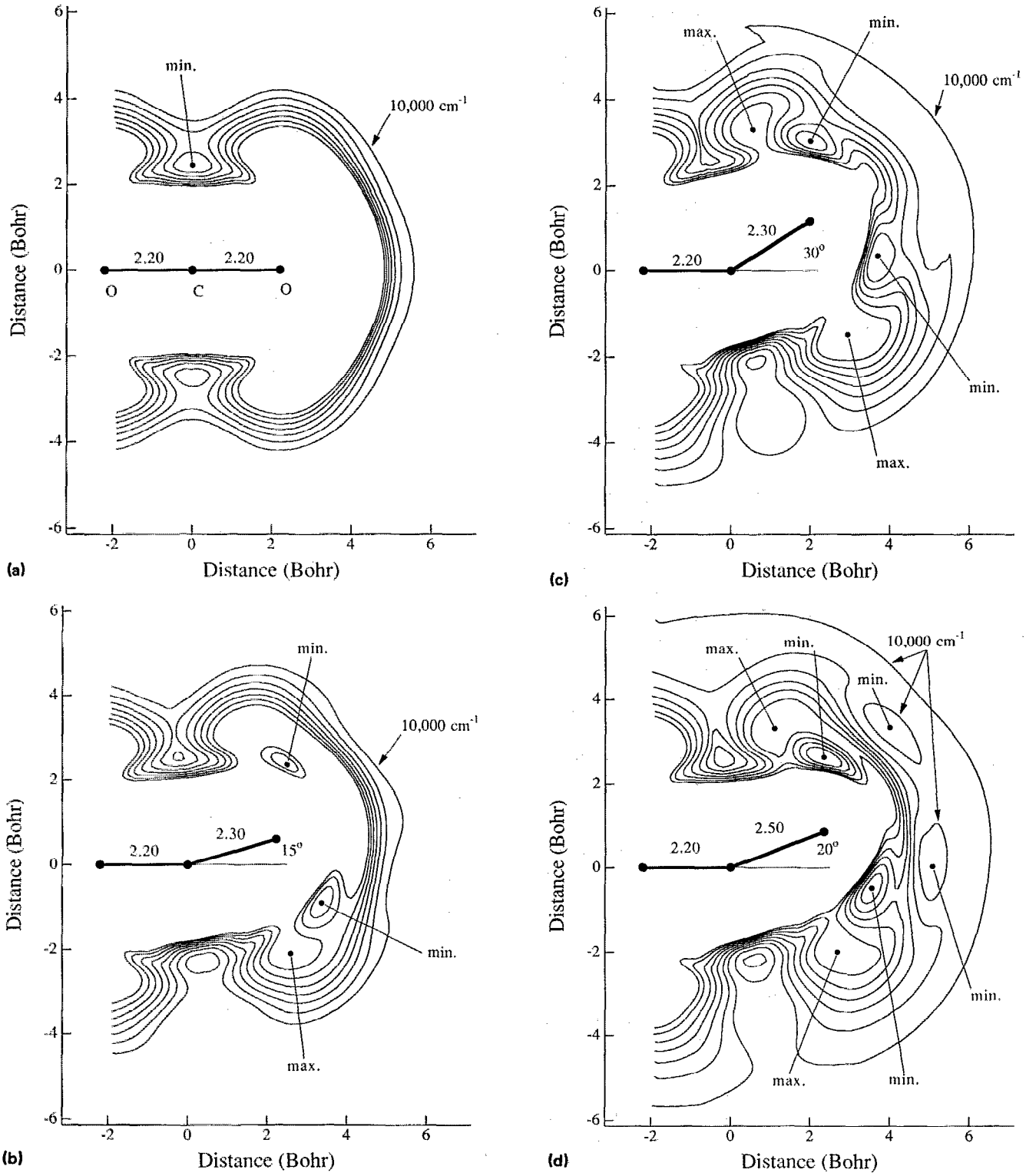

FIG. 6. H-atom energy contours for several OCO geometries: (a) the equilibrium geometry of free CO_2; (b) $\theta_{OCO} = 165°$, $R_{CO} = 2.30$ bohr; (c) $\theta_{OCO} = 150°$, $R_{CO} = 2.30$ bohr. (d) *Cis* saddle point geometry; $\theta_{OCO} = 160°$, $R_{CO} = 2.50$ bohr. Contours are separated by 2500 cm^{-1}; the highest is at 25 000 cm^{-1}.

available to product degrees of freedom is $\sim 10\,000\ cm^{-1}$, of which an average of $\sim 1500\ cm^{-1}$ appears as CO internal excitation. The rotational surprisal parameters of $\theta_R = 7$ and 9, for $v = 0$ and 1, respectively, indicate that the rotational distribution is colder than expected from a statistical (i.e., $\theta_R = 0$) distribution of the available energy.

In previous studies, nascent OH rotations were found to be colder than statistical;[2-4] e.g., for 193 nm HBr photolysis, the OH($v = 0$) average rotational energy is $\sim 1350\ cm^{-1}$ (Ref. 4). In addition, Hoffmann *et al.* measured the CM kinetic energy using sub-Doppler techniques following 193 nm HBr photolysis, obtaining an average CM kinetic energy of $\sim 9800\ cm^{-1}$ for several OH($v = 0$,low-J) levels.[10] When monitoring a specific OH(v,J) level, the energy available to the remaining 6 degrees of freedom is given by $h\nu - D_0(HBr) - E_{int}(OH)$, and in the Chen *et al.* experiments $E_{int}(OH)$ was small. Thus the CM kinetic energy averaged over the entire ensemble of OH product states will be lower than $9800\ cm^{-1}$. An exact comparison cannot be made between these previous studies and the present work, since 193 nm HBr photolysis provides more energy than does 193 nm H_2S photolysis. However, it is clear that energy is released preferentially into CM kinetic energy.

Although diode laser probing of CO leads to larger fluctuations in the rotational distributions than with probes such as LIF and MPI, distinguishing gain from absorption is easy. Thus determining whether the $[v = 1]/[v = 0]$ ratio is larger or smaller than unity is straightforward unless the level densities are close or the $v = 0$ and 1 rotational distributions differ markedly. As stated above, we observe only absorption on $1 \leftarrow 0$ and $2 \leftarrow 1$ transitions and find essentially no signals for $3 \leftarrow 2$ transitions. It is unlikely that the $v = 2$ and 3 populations are such that there is fortuitously no population difference for the probed rotational levels. Thus we conclude that vibrational excitation is modest, with $[v = 1] < [v = 0]$ and little or no population at $v \geqslant 2$.

Only approximate rotational distributions could be obtained from the data because of limited S/N and the fact that CO transitions were accessible one at a time within each of the single-mode diode laser tuning curves. Lack of population at $v \geqslant 2$ in consistent with all other measurements, and our $[v = 1]/[v = 0]$ ratio of ~ 0.4 agrees with that of Weston and co-workers,[15] but disagrees with that of Rice *et al.*[7] Our $v = 0$ rotational distribution agrees with theirs, but their $v = 1$ rotational distribution shows an inversion while ours does not. Their data have reasonable S/N and the distributions derive from straightforward analyses, so we assume the difference is real. It can be traced to their $v = 1$ high-J population, which accounts for the comparable $v = 0$ and 1 populations as well as the inversion. In our experiments, there is some rotational relaxation, so we cannot rule this out as a means of reconciling the different $v = 1$ rotational distributions. However, this would require a large change in our $v = 1$ rotational distribution, so we believe that there is no rotational inversion. Also, $[v = 1]/[v = 0] \sim 0.4$ was confirmed under conditions where rotational relaxation was considered complete. There is no way that we can get $[v = 1] = [v = 0]$ from our data.

Our estimate of CO internal energy suggests a bias in which CO internal excitation is less than statistical, a conclusion also reached by Rice *et al.* The calculations of Schatz *et al.*[8(a)] at a collision energy of 2.6 eV indicate somewhat more internal excitation, although it is not clear how much of this

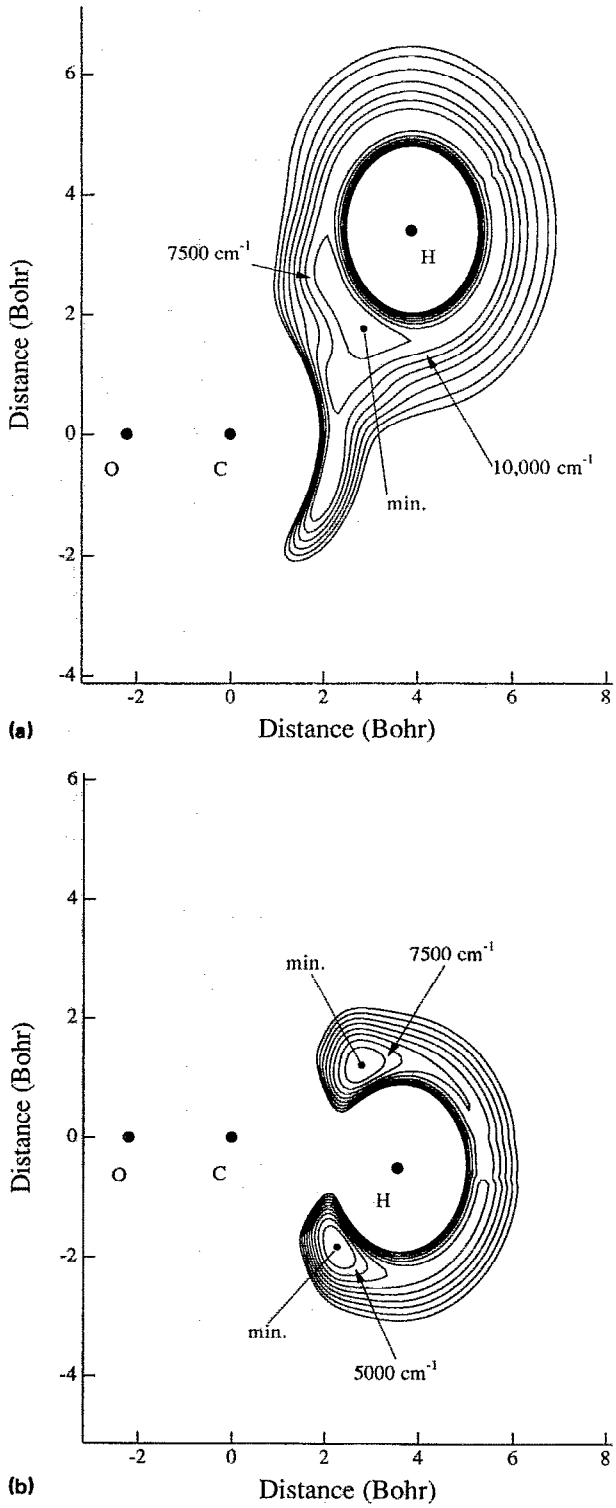

FIG. 7. O-atom contours for fixed O, C, and H positions: (a) H atom at *cis* saddle point; (b) H atom at minimum of *trans* well in Fig. 6(d). Contours are separated by $2500\ cm^{-1}$.

is due to classical vs quantum differences. Combined with the earlier measurements of OH internal states and CM kinetic energy, the composite picture is that at high collision energies there is a propensity toward CM kinetic energy at the expense of product internal excitations.

Insight into the dynamics can be gained by examining the HOCO potential energy surface. Figure 6 shows H atom energy contours at several fixed OCO geometries. For the OCO nuclei held at the CO_2-molecule equilibrium geometry, the closest thing to an attractive well is a shallow minimum along a broadside C_{2v} approach to the C atom [Fig. 6(a)]. As the OC–O bond is bent and stretched, attractive wells at the *cis* and *trans* positions begin to form, deepening with increasing angle [Figs. 6(b) and 6(c)]; the lowest energy reaction pathway is for *cis* HOCO [Fig. 6(d)]. It is clear that the OC–O bond must be bent and stretched from its equilibrium position for the H atom to be trapped on the HOCO surface. There are, however, only a limited number of approaches that will produce the changes in the OC–O geometry necessary to effect chemical reaction, the majority of collisions resulting in elastic or inelastic scattering. However, in those collisions that lead to reaction, the H atom is left in the *trans* instead of the lower energy *cis* position. The result is a dynamical barrier. This is consistent with the low reaction probability of 0.024 estimated at $E_{CM} = 2.4$ eV,[15] as well as the variation of reaction probability with collision energy reported earlier.[9]

A second feature of the HOCO intermediate becomes apparent when forces on the reacting O atom are examined by moving the O atom while holding the other atoms fixed. The light H atom will not remain stationary while the heavy O atom lumbers about. On the contrary, rapid H-atom motion will result in an average potential acting to expand the OC–OH bond. Figure 7 shows the O atom potential at two different geometries: (a) places the H atom at the calculated geometry of the *cis* saddle point while (b) places the H atom at the bottom the *trans* well of the potential shown in Fig. 6(d). In each case, the forces push the O atom away from the CO. Similar results were found for other H atom configurations.

Much past experimental work has been interpreted in terms of reactants that form a $HOCO^{\dagger}$ intermediate that lives for many vibrational periods before proceeding to products. Indeed, the measurements of Scherer *et al.* seem to confirm this by showing that it takes a few picoseconds for OH to appear following photoexcitation of CO_2–HI complexes.[6] To the extent that these measurements can be interpreted in terms of $H + CO_2$ collisions, they underscore the role of a $HOCO^{\dagger}$ intermediate. However, whether intramolecular vibrational redistribution (IVR) can be complete on so short a time scale is another question. In fact, estimates of unimolecular decay lifetimes for the high E_{CM} values used in the present studies, based on standard statistical theories that assume complete IVR, yield values under 1 ps.[10] Furthermore, a distinction must be made between experiments performed under bulk conditions and those involving weakly bonded complexes. With the latter, the Br or I atom may remain near HOCO and influence the reaction. Thus bulk and complex reactions may be mechanistically different.

V. SUMMARY

Modest CO internal excitation is observed and was anticipated on the basis of previous measurements of OH V,R excitation and CM kinetic energy.[4,5,10] This confirms that high collision energies favor product CM kinetic energy at the expense of internal excitations. The CO internal energy of $\sim 1500\ cm^{-1}$ is $\sim 15\%$ of the available energy, and the $v = 0$ and 1 rotational distributions are much colder than statistical. Our $v = 0$ rotational distribution agrees with that of Rice *et al.*,[7] while our $v = 1$ rotational distribution differs from theirs. Ours is qualitatively similar to that of $v = 0$, while theirs shows substantial high-J population. We detect absorption when probing a large number of $1 \leftarrow 0$ transitions (i.e., $0 \leqslant J \leqslant 50$), while the Rice *et al.* distribution would result in gain for a broad range of J values. Despite this difference, both sets of data indicate that CO internal excitation is less than statistical. Examination of the HOCO potential suggests a dynamical barrier, i.e., collisions that move the OCO nuclei to a reactive configuration do not leave the system near the lowest energy reaction path.

The observed dynamical features, as manifest in nascent product excitations, constitute an example of nonstatistical behavior in a system undergoing reaction on a potential with a prominent minimum, in this case corresponding to the HOCO intermediate.[8] However, product state distributions are only part of the story. By themselves they do not permit conclusions to be drawn about the completeness of IVR. Also, what about rates? At the high collision energies where product state distributions are nonstatistical, RRKM theory cannot be applied because the IVR rate might not exceed the reaction rate, a necessary condition for the theory to hold. For example, RRKM estimates of reaction rates at energies $\sim 12\,000\ cm^{-1}$ above the OH + CO channel are near $10^{13}\ s^{-1}$,[10] out of the range where the theory applies. Also, it is at these high energies where the reaction cross section rises steeply with increasing collision energy.[9] Experiments like those of Żewail and co-workers, in which CO_2–HI complexes are excited and OH is detected, enable the OH temporal buildup to be determined with subpicosecond resolution.[6] In their experiments, buildup times of several ps were noted, much longer than calculated from statistical theories. To the extent that such measurements can be related to the corresponding $H + CO_2$ reaction, it may be possible to determine reaction rates directly in the high energy regime, thus elucidating reaction mechanisms.

ACKNOWLEDGMENT

Research supported by the U.S. Army Research Office, Center for the Study of Fast Transient Processes.

[1] C. R. Quick and J. J. Tiee, Chem. Phys. Lett. **100**, 223 (1983).
[2] K. Kleinermanns, E. Linnebach, and J. Wolfrum, J. Phys. Chem. **89**, 2525 (1985).
[3] A. Jacobs, M. Wahl, R. Weller, and J. Wolfrum, Chem. Phys. Lett. **158**, 161 (1989).
[4] G. Radhakrishnan, S. Buelow, and C. Wittig, J. Chem. Phys. **84**, 727 (1986).
[5] J. Rice, G. Hoffmann, and C. Wittig, J. Chem. Phys. **88**, 2841 (1988).
[6] N. F. Scherer, L. R. Khundkar, R. B. Bernstein, and A. H. Zewail, J. Chem. Phys. **92**, 5239 (1990).

[7](a) J. K. Rice, Y. C. Chung, and A. P. Baronavski, Chem. Phys. Lett. **167**, 151 (1990); (b) J. K. Rice and A. P. Baronavski, J. Chem. Phys. **94**, 1006 (1991).
[8](a) G. C. Schatz, M. S. Fitzcharles, and L. B. Harding, Faraday Discuss. Chem. Soc. **84**, 359 (1987); (b) M. Aoyagi and S. Kato, J. Chem. Phys. **88**, 6409 (1988).
[9]Y. Chen, G. Hoffmann, D. Oh, and C. Wittig, Chem. Phys. Lett. **159**, 426 (1989).
[10]G. Hoffmann, D. Oh, Y. Chen, and C. Wittig, Isr. J. Chem. (1989).
[11]B. Lewis and G. von Elbe, in *Combustion, Flames and Explosions of Gases* (Academic, Orlando, 1987), p. 78.
[12]M. Mozurkewich, J. J. Lamb, and S. W. Benson, J. Phys. Chem. **88**, 6435 (1984).
[13]Z. Xu, B. Koplitz, and C. Wittig, J. Chem. Phys. **87**, 1062 (1987).
[14]J. Wolfrum (private communication).
[15]R. E. Weston (private communication).
[16](a) J. O. Chu, C. F. Wood, G. W. Flynn, and R. E. Weston, J. Chem. Phys. **81**, 5533 (1984); (b) J. A. O'Neill, J. Y. Cai, G. W. Flynn, and R. E. Weston, *ibid.* **84**, 50 (1986); (c) J. A. O'Neill, C. X. Wang, J. Y. Cai, G. W. Flynn, and R. E. Weston, Jr., *ibid.* **88**, 6240 (1988).
[17]P. Roth, R. Loehr, and U. Barner, Combust. Flame **45**, 273 (1982).
[18]G. Hancock and I. W. M. Smith, Appl. Opt. **10**, 1827 (1971).
[19]R. D. Levine and R. B. Bernstein, Acc. Chem. Res. **7**, 393 (1974).
[20]S. K. Shin, Y Chen, S. Nickolaisen, S. W. Sharpe, R. A. Beaudet, and C. Wittig, in *Advances in Photochemistry, Vol. 16*, edited by D. Volman, G. Hammond and D. Neckers (Wiley, New York, 1991).